Article:
Makris, K.F., Langeveld, J.G., Clemens-Meyer, F.H.L.R. et al. (3 more authors) (2022) Sonic assessment of physical ageing of plastic pipes. Journal of Sound and Vibration, 544. 117393. ISSN 0022-460X

https://doi.org/10.1016/j.jsv.2022.117393

Journal of Sound and Vibration 544 (2023) 117393

Contents lists available at ScienceDirect

Journal of Sound and Vibration

journal homepage: www.elsevier.com/locate/jsvi

Sonic assessment of physical ageing of plastic pipes

Konstantinos F. Makris [a,*], Jeroen G. Langeveld [a,b], François H.L.R. Clemens-Meyer [c,d], Joanna Watts [e], Hasina Begum [e], Kirill V. Horoshenkov [e]

[a] Department of Watermanagement, Faculty of Civil Engineering and Geosciences, Delft University of Technology, Stevinweg 1 (Building 23), 2628CN Delft, The Netherlands
[b] Partners4UrbanWater, Graafseweg 274, 6532 ZV Nijmegen, The Netherlands
[c] Norwegian University of Science & Technology, Faculty of Engineering, Department of Civil & Environmental Engineering, Vassbygget, 422, Vallgrinda, S.P. Andersens veg 5, Trondheim, Norway
[d] Department of Hydraulic Engineering, Deltares, Boussinesqweg 1, 2629HD, Delft, The Netherlands
[e] Department of Mechanical Engineering, University of Sheffield, S1 3JD Sheffield, United Kingdom

ARTICLE INFO

Keywords:
Acoustic waves
Ageing
Storage modulus
Fluid-filled pipe
Wave propagation
Dispersion equation

ABSTRACT

This article explores the potential of vibro-acoustics to detect physical ageing of plastic pipes. For this purpose, two different topics are combined: the ability of vibro-acoustics to estimate the storage modulus of a plastic pipe, and the sensitivity of the estimated storage modulus to changes due to ageing. Concerning the first topic, a vibro-acoustic method was applied to two water-filled HDPE pipes, one surrounded by air and another by sand. The excitation was achieved via an impact hammer and the propagating signal was recorded with the aid of hydrophones. Signal analysis led to the estimation of the axial wavenumber of the propagating axisymmetric fluid-borne wave. This value was used in the dispersion equation for the propagating mode to evaluate the storage modulus of the pipe material for a given experimental setup. Results revealed that the vibro-acoustic method gives consistent and reliable estimations of the storage modulus. Concerning the second topic, samples from two PVC pipes with an age difference of 41 years were subjected to dynamic mechanical analysis to study the behaviour of the storage modulus as a function of frequency. Results showed that it is feasible to distinguish discrepancies in the magnitude of the storage modulus due to ageing, provided that the measurement uncertainty is small. The uncertainty analysis highlighted the parameters that need to be more accurately known in order to lower the overall uncertainty of the estimated storage modulus when the proposed vibro-acoustic method is used. Irrespectively of the medium surrounding the pipe (air or soil), the distance between the points of the recording signals should be sufficiently long to measure the signal phase accurately. It was found that the accurate knowledge of the pipe's geometry, i.e. the wall thickness and internal radius, was more or equally important for controlling the overall uncertainty than that of the parameters of surrounding soil.

1. Introduction

Physical ageing is considered as one of the profound degradation mechanisms of plastic pipes used in water [1] and gas [2] distribution systems, and in urban drainage systems [3]. Tensile testing indicates that ageing imposes an increase in the ultimate stress, followed by a decrease in the strain at break. Ageing is also well correlated with an increase in the elastic modulus. Plastic

* Corresponding author.
E-mail address: k.makris@tudelft.nl (K.F. Makris).

https://doi.org/10.1016/j.jsv.2022.117393
Received 11 June 2022; Received in revised form 26 September 2022; Accepted 19 October 2022
Available online 25 October 2022

(i.e. PVC) pipes that have been in service for approximately 4 decades have demonstrated an increase in elastic modulus up to 37% [3]. This transition towards more brittle material behaviour due to ageing is also reflected on the lower impact resistance [4,5]. Consequently, potential issues should be considered regarding the stability of the pipe during inspection, activities in the close vicinity and the installation of new household connections.

Besides conventional tensile testing [1,3] and impact tests [4,5], other methods have also been utilized in order to study physical ageing in thermoplastic materials. Most existing methods are destructive, such as differential scanning calorimetry [5], dynamic mechanical analysis [5,6], and tensile/ torsional creep compliance measurements [4,7]. However, the development of non-destructive single-sided (from the pipe's interior) techniques is essential to inspect pipes in operation to ensure lower inspection costs and minimal disruption of the system. Relevant studies explore the capabilities of micro-indentation [1] and non-collinear ultrasonics in ageing detection [8,9]. Nonetheless, significant limitations exist in both methods, since micro-indentation focuses only on the surface of the material, while non-collinear ultrasonics require continuous precise alignment and known acoustic properties of the inspected medium. A common way to estimate the linear properties of materials in the lower strain non-destructive regime is ultrasound [10,11]. However, the capability of detecting ageing at high ultrasonic frequencies has proved to be challenging [7]. As a result, the measured sound velocity of the material, and relatedly the storage modulus, is insensitive to ageing for frequency values within the ultrasonic domain with the conventional pulse-echo method [8].

So far, there is no recorded attempt to track a pipe's storage modulus with low frequency acoustics. The term "low frequency" in acoustics denotes frequencies at which the compressional wavelength in the pipe wall is larger than the inner circumference of the pipe [12]. Apart from higher sensitivity to ageing, a shift to lower frequencies would also limit the number of propagating acoustic modes mainly to the axisymmetric. These are the longitudinal L(0,1) and torsional T(0,1) modes. For fluid-filled pipes, an additional mode, the fluid-borne wave, can also be detected at low frequencies. In the literature, the fluid-borne mode has received much attention since it attenuates significantly less compared to the other modes when the pipe is buried and it is less affected by the presence of joints and fittings [13]. Application of the fluid-borne wave has been studied mainly in order to locate the position of a leakage in water distribution systems via correlation of the received signals from the leakage at two known locations and corresponding time delay [14,15]. Other applications of axisymmetric waves include the estimation of soil parameters around the pipe [16] and locating buried pipes via ground surface vibration [17]. These waves can be excited in-situ with a relatively complex experimental set-up [18,19].

In this article, a new method to track the ageing levels of plastic pipes is proposed based on low frequency vibro-acoustics. An impact hammer was used to excite low frequency waves in water-filled high-density polyethylene (HDPE) pipes installed above and below ground. The propagated wave signal was received on the hydrophones inserted in the pipe. The raw signals were processed to estimate the real part of the axial wavenumber of the propagating fluid-borne wave. Subsequently, the complete dispersion equation for axisymmetric waves (Appendix A) was applied to the experimental data to estimate the storage modulus of the pipe material. Dynamic mechanical analysis (DMA) was carried out on samples from the HDPE pipes to verify the magnitude of the estimated storage modulus. DMA was also conducted on samples taken from PVC pipes with extrusion age difference of 41 years to study how the storage modulus behaves with respect to frequency and pipe age. This enables us to suggest that the axisymmetric fluid-borne wave can be used to detect ageing of buried plastic pipes.

2. Methodology

2.1. Experimental setup

Two different setups were used to examine the propagation of the fluid-borne wave in a water-filled HDPE pipe surrounded by air ("Set-up A") and water-filled HDPE pipe surrounded by sand ("Set-up B"). These pipes had an external diameter of 110 mm and wall thickness of 11 mm and were installed in a 40 m long, 3 m wide and 5 m deep sandpit in the The Integrated Civil and Infrastructure Research Centre at the University of Sheffield. The excitation of waves in the system was achieved via an impact hammer (PCB 086C03, 0.16 kg). The rubber tip of the hammer was carefully selected to generate low frequency modes of interest. A built-in load cell connected to the tip of hammer was capable of recording the force applied to the pipe at every hit. The acoustic signal was captured with hydrophones (B&K 8103) connected to a condition amplifier (B&K Nexus 2693-0S4). Fig. 1 shows the two experimental setups including the hydrophone arrangements in the pipes. Set-up A was a straight pipe (see Fig. 1(a)). In this set-up, just one hydrophone was used as the distance between the excitation point and hydrophone could be directly measured 5.3 m. Set-up B was a combination of a straight section and elbow section tilted at an angle (see Fig. 1(c)). In this set-up a second hydrophone was added 0.3 m away from the first one to help to resolve the uncertainty in the measurement of the effective distance between the impact and receiver points. The detected vibration and acoustic signals were recorded with a data acquisition module (NI USB-4431) at the sampling rate of 12 kHz.

The measured or assumed values and their standard deviations in the properties of the pipe material, water and soil are given in Table 1. The density of the pipe material was measured from extracted samples according to ISO 1183-1 [20] (immersion method) and was found to be 957.6 kg/m^3. The geometry of the pipe shell (wall thickness and internal radius) was determined in-situ with a measuring tape, accepting an uncertainty of 0.5 mm. Regarding the properties of water, reported values were used [21] with suitable uncertainties to compensate for temperature changes within a certain temperature range (10 –20 °C). The values of the remaining properties were retrieved from literature. The magnitude of their uncertainties was based on the variability of the values observed in different scientific sources [17,22–24] and expected variability in practice, rather than the prevailed laboratory conditions in the current study.

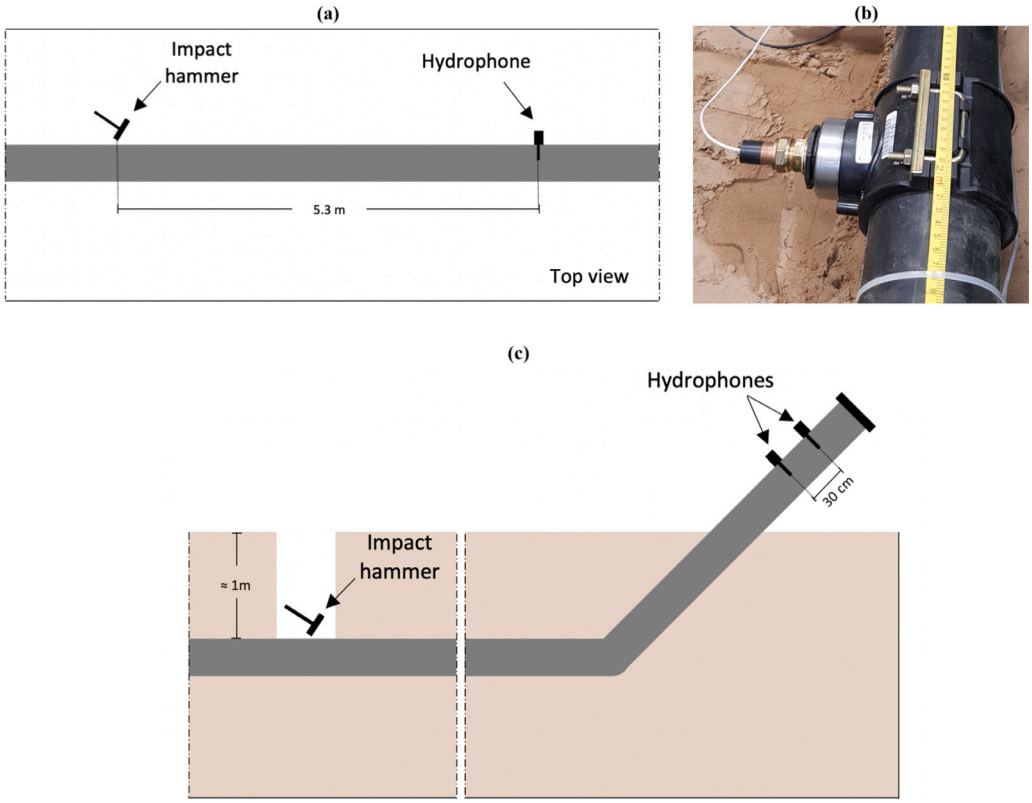

Fig. 1. An illustration of the experimental set-ups: Set-up A (a); hydrophone installation method (b); and Set-up B (c).

Table 1
Measured or assumed pipe, water and soil properties and their standard uncertainties used in the following analyses.

Medium	Property	Symbol (Units)	Value	Uncertainty
Pipe shell	Density	ρ (kg/m^3)	957.6	1.4
	Poisson ratio	υ (-)	0.4	0.05
	Loss factor	η_s (-)	0.05	0.01
	Internal radius	R_i (mm)	44	0.5
	Wall thickness	h (mm)	11	0.5
Fluid	Density	ρ_f (kg/m^3)	998	2
	Compressional wave velocity	c_f (m/s)	1481.4	35
Soil	Density (bulk)	ρ_s (kg/m^3)	1500	600
	Compressional wave velocity	c_d (m/s)	200	150
	Shear wave velocity	c_t (m/s)	100	28

The soil in the below-ground section was washed silica sand and assumed properties were retrieved from Gao et al. [17]. The uncertainties of the soil parameters were considered higher compared to these of other media, since soil is expected to be the medium with the highest parameter variability. These uncertainties can be high enough for the density and sound speeds to be comparable with the values reported by Long et al. [25] ($\rho_s = 2100$ kg/m^3, $c_d = 350$ m/s and $c_t = 70$ m/s) for typical sandy soil.

2.2. Signal analysis

Fig. 2 presents the process that was followed to estimate the real part of the axial wavenumber k_z^{re} of the fluid-borne mode from the raw signals. Depending on the set-up, raw signals could refer to signals from the impact hammer and single hydrophone (Set-up A) or exclusively to signals from the two hydrophones (Set-up B). A Hanning time window was applied to the signals in order to isolate the desired mode (i.e. the fluid-borne wave) from other present modes or signals reflected from various artefacts. The Hanning window was selected as it ensures the smoothing of abrupt ends and reduction of the spectral leakage. The application of a 6th order bandpass Butterworth frequency filter allowed for the analysis in a specific frequency range. The selected order of the filter proved to provide a numerically stable output signal with a flat magnitude response between the cut-off frequencies. The choice of the cut-off frequencies (f_b and f_e) was informed by the coherence analysis of the raw signals to help identify the frequency

range in which the two recorded signals were linearly related. As a result, the cut-off frequencies for the analysis of each set-up were determined by observing the consistent tendency of the coherence function to approach unity. The coherence is defined as [26]:

$$\gamma(\omega) = \frac{|G_{12}(\omega)|^2}{|G_{11}(\omega)||G_{22}(\omega)|} \tag{1}$$

where G_{12} is the mean cross-spectral density between the two signals, G_{11} and G_{22} are their mean autospectral densities, and ω is the angular frequency.

The transition to the frequency domain was achieved by applying the Discrete Fourier Transform (DFT) to each signal and then extracting the phase. The real axial wavenumber was estimated on the basis of the difference in the phase between the two signals and distance between the points of their reception. In total, the experiments were repeated 10 times for each experimental set-up and recorded spectra were averaged for the analysis.

2.3. Pipe storage modulus estimation

The storage moduli of the pipes in the described experimental setups were estimated by solving the complete dispersion equation for sound propagation in a water-filled visco-elastic pipe in vacuum (used for Set-up A) or buried in soil (used for Set-up B). Appendix A presents the derivation of the general solution (Eq. (A.23)) and solution specific for the axisymmetric modes (Eq. (A.24)). Rearranging Eq. (A.24) with respect to the pipe's storage modulus E leads to the function f of various properties:

$$E = f(v, \rho, \eta_s, R_i, h, \rho_f, c_f, \rho_s, c_d, c_t, k_z^{re}, k_z^{im}) \tag{2}$$

where k_z^{re} and k_z^{im} are the real and imaginary part of the axial wavenumber, respectively, and the rest of the symbols are defined in Table 1. In the case of Set-up A, the soil related parameters were ignored in this analysis.

When putting this methodology into practice, the use of the Law of Propagation of Uncertainties (LPU) is essential in order to define the uncertainty levels of the estimated storage modulus. Assuming that all the parameters in Eq. (2) are considered independent and therefore all the covariances are zero, the combined effect of the individual standard uncertainties can be expressed via the LPU [27]:

$$u(E)^2 = \sum_{n=1}^{N} u(x_i)^2 \left(\frac{\partial f}{\partial x_i}\right)^2 \tag{3}$$

where $u(x_i)$ is the standard uncertainty of each individual parameter x_i and N is the total number of parameters in the function f in Eq. (2).

The individual uncertainties in Eq. (3) are known for all the parameters (Table 1) except for the components of the axial wavenumber (k_z^{re} and k_z^{im}). The application of the LPU to the formula for the real part of the axial wavenumber k_z^{re} (Fig. 2) allows for the estimation of its standard uncertainty $u(k_z^{re})$ (assuming independent measurements) [27]:

$$u(k_z^{re}) = \sqrt{\frac{1}{dz^2}u^2(d\phi) + \frac{d\phi^2}{dz^4}u^2(dz)} \tag{4}$$

where dz is the distance between the two considered sensors (impact hammer and/or hydrophone(s)), $u(dz)$ is the uncertainty of the distance dz, $d\phi$ is the phase difference between the received signals, and $u(d\phi)$ is the uncertainty of the phase difference $d\phi$. $u(dz)$ was assumed to be 0.5 mm and $u(d\phi)$ was estimated as the standard deviation in the phase measured across all the experiments for a given set-up.

Further, the presented signal analysis offers a process to extract only the real part of the axial wavenumber (k_z^{re}). In this study, the imaginary part k_z^{im} was difficult to extract accurately from the experiments and it was considered to be zero irrespectively of frequency. In order to evaluate the effect of this choice, the two setups were simulated in COMSOL Multiphysics®. Subsequently, the uncertainty of the imaginary part of the axial wavenumber was considered to be equal to the value of the imaginary part itself ($u(k_z^{im}) = k_z^{im}$). Details on the development of the models along with the solutions are given in Appendix B.

2.4. Dynamic mechanical analysis and ageing

Dynamic mechanical analysis (DMA) was performed in order to study the viscoelastic behaviour of samples taken from the HDPE pipes used in the described experiments and from two PVC pipes extensively tested by Makris et al. [3]. The samples were milled along the longitudinal pipes axis and through the whole pipe wall thickness. The sample dimensions were 20 mm x 10 mm x 11 mm for the HDPE samples and 20 mm x 10 mm x 8 mm for the PVC samples. The desired parameter was the frequency-dependent storage modulus of the pipe material. DMA was conducted with a Metravib (VA 2000) analyzer at frequencies between 1 and 50 Hz, within a temperature range of −10 °C to 20 °C at 5 °C steps. Subsequently, time–temperature superposition was applied in order to estimate the storage modulus at a wider range of frequencies and specific reference temperature (10 °C for the HDPE pipe in lab conditions and 20 °C for the PVC samples).

In the case of the HDPE pipes, the storage modulus from DMA was compared to the storage modulus calculated from the vibro-acoustic method. In the case of the PVC pipes, the storage modulus from DMA was used to explore the capability of the fluid-borne axisymmetric wave to detect physical ageing at low frequencies while considering the uncertainty levels measured from the actual vibro-acoustic experiments. The measured uncertainty of the storage modulus for the two different setups was expressed as a percentage which was thereafter applied to the modulus values obtained from the DMA results. The PVC pipes were a 44 years old pipe ("P-1") that had served as a foul sewer and a 3 years old unused pipe ("P-2").

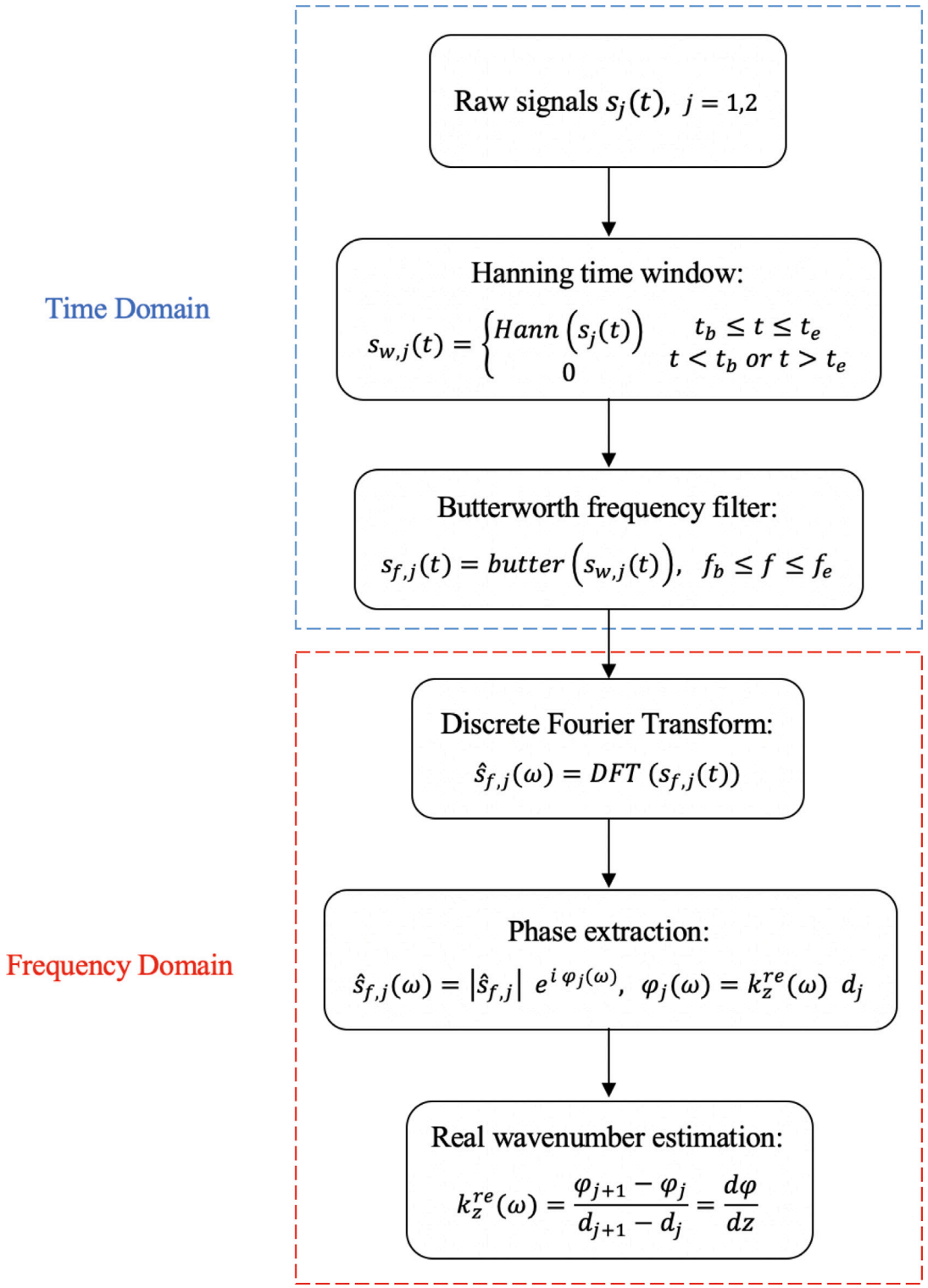

Fig. 2. The flowchart of the process used to estimate the real wavenumber k_z^{re} from the raw signals. The subscripts "b" and "e" denote the upper and lower limits in time windowing and frequency filtering. ϕ_j is the extracted phase of a signal, d_j is the distance between the excitation point and the point of signal reception, $d\phi$ and dz are the phase difference and distance between two receiving signals respectively, and $i = \sqrt{-1}$.

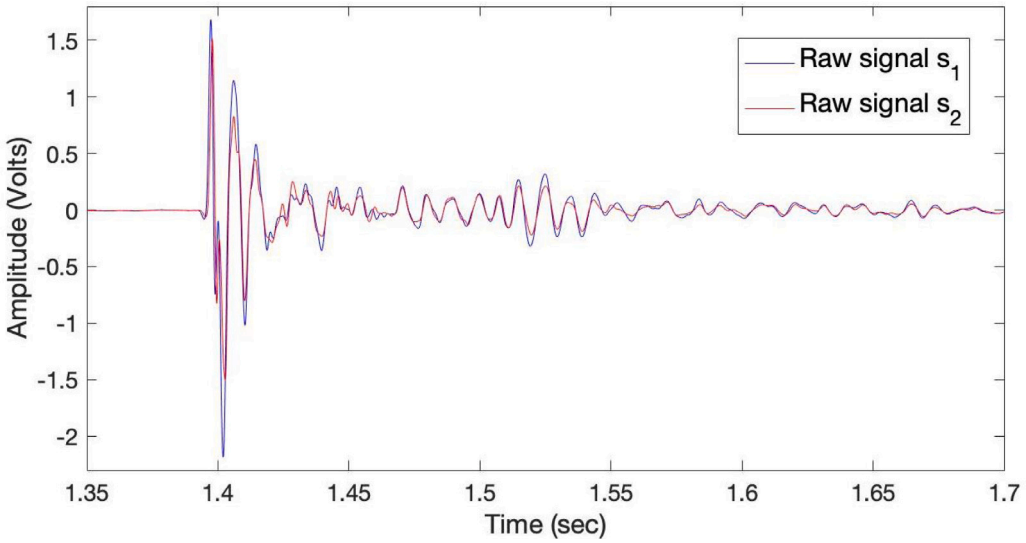

Fig. 3. An example of raw signals, s_1 and s_2, received on the two hydrophones in Set-up B.

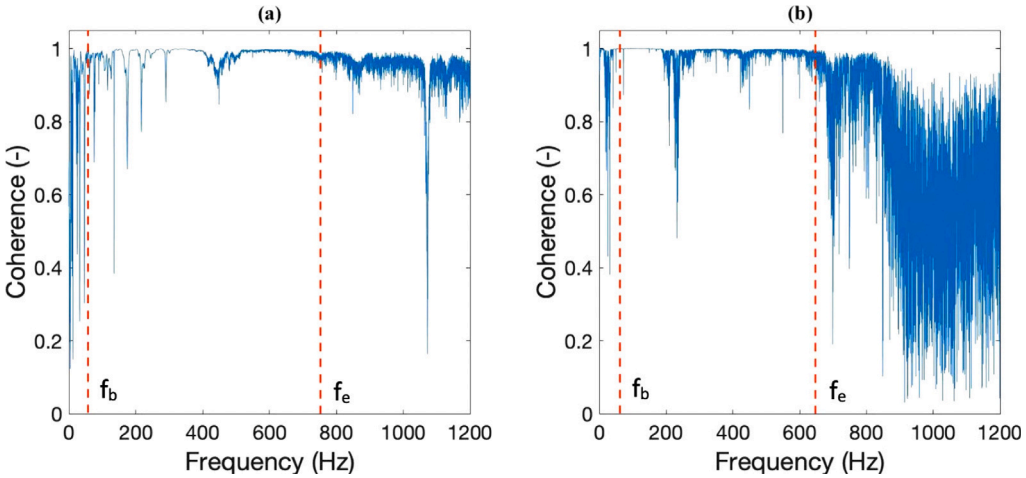

Fig. 4. The coherence as a function of frequency between the hammer and the single hydrophone signal in Set-up A (a) and between the two hydrophone signals Set-up B (b). In each case, the coherence is estimated from Eq. (1). The red dashed lines show the frequencies f_b and f_e used in the Butterworth frequency filter.

3. Results

3.1. Estimation of the pipe storage modulus using vibro-acoustics

An example of the received raw signals from the two hydrophones in Set-up B is given in Fig. 3. With such raw signals, the coherence for a wide range of frequencies (up to 6 kHz) was determined for both setups (Fig. 4). The presented coherence values were evaluated based on the average cross-spectral and auto-spectral densities of the signals received during ten repeated independent measurements.

A Hanning time window was applied to the raw signal. The shape and extent of the time window is presented in Fig. 5(a). Fig. 5(b) presents an example of its application on the raw signals. The frequency limits used for the Butterworth frequency filtering of the signals were determined at the points in which the coherence function deviated consistently from unity as illustrated in Fig. 4. Following the notation given in Fig. 2, f_b and f_e were set to 50 and 750 Hz, respectively, for Set-up A, and 50 and 650 Hz for Set-up B.

Fig. 6 presents the real part of the wavenumber of the axisymmetric fluid-borne mode for Set-up A and Set-up B. The mean value represents the average of 10 experiments and the 95% confidence interval is twice the uncertainty calculated via Eq. (4). Set-up B demonstrates a lower mean wavenumber (or higher mean phase velocity) within the examined frequency range, which indicates

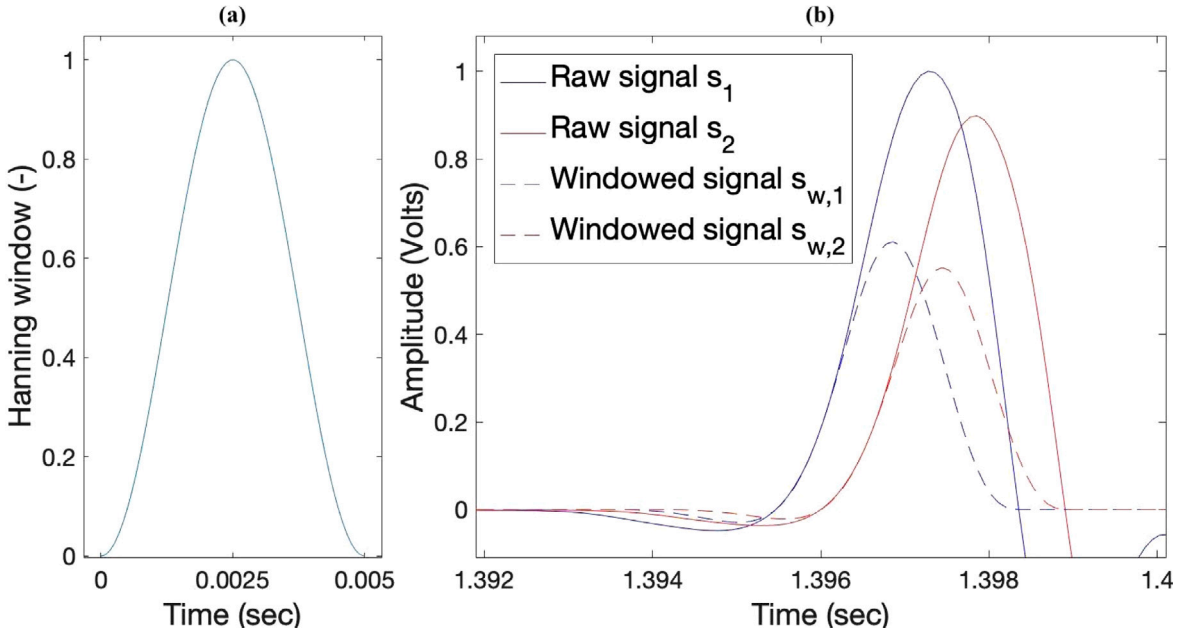

Fig. 5. (a) The Hanning window used in the processing of raw signals according to the procedure described in Fig. 2. (b) Example of windowed signals $s_{w,1}$, $s_{w,2}$ after applying the Hanning window to raw signals s_1, s_2.

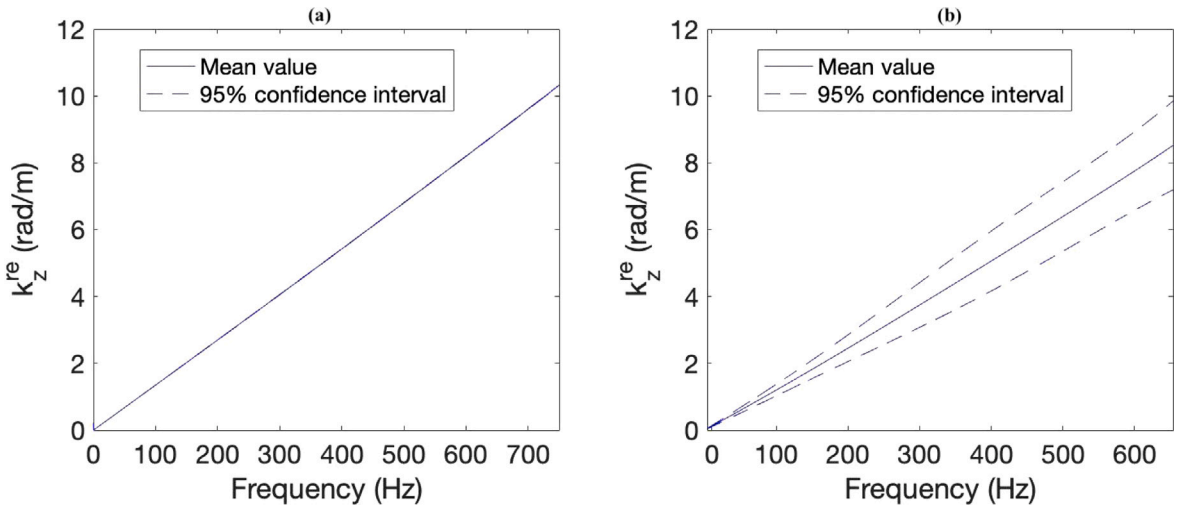

Fig. 6. The real part of the axial wavenumber k_z^{re} as a function of frequency for Set-up A (a) and Set-up B (b). k_z here represents the wavenumber of the axisymmetric fluid-borne wave. The results were obtained by processing the raw signals according to the procedure described in Fig. 2.

the added stiffness from the surrounding soil. Further, the results for Set-up B show relatively wider confidence intervals, which imply higher uncertainty levels compared to Set-up A.

The values of the storage modulus estimated from the vibro-acoustic data and respective uncertainty levels (95% confidence interval) are depicted in Fig. 7. Irrespectively of the used set-up, the mean value of the storage modulus lies around 2.2 GPa within the considered frequency range. The results from the pipe section buried in sand show a relatively high uncertainty which is frequency dependent with the maximum between 200 and 400 Hz.

3.2. Estimation of the pipe storage modulus based on DMA

Fig. 8 presents the storage modulus for the HDPE sample measured with the DMA method. Fig. 8(a) shows the dependence of the modulus as a function of temperature for the range of frequencies used in DMA. Fig. 8(b) shows the frequency-dependent storage

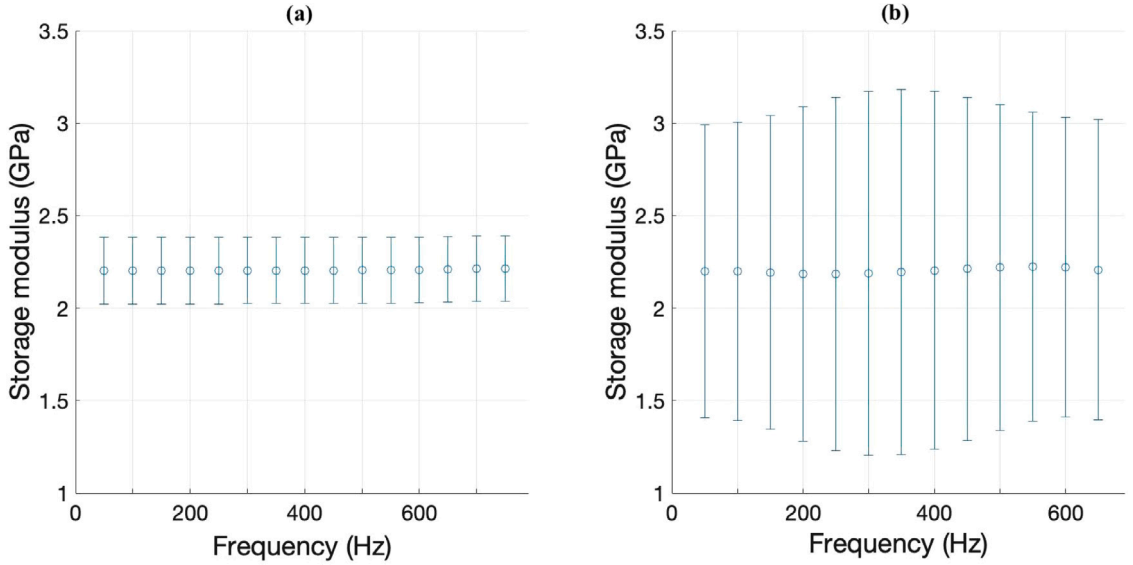

Fig. 7. The estimated pipe storage modulus as a function of frequency for Set-up A (a) and Set-up B (b). The error bars denote the 95% confidence interval. The results are based on the parameters given in Table 1 and Eq. (A.24) derived for the axisymmetric fluid-borne wave.

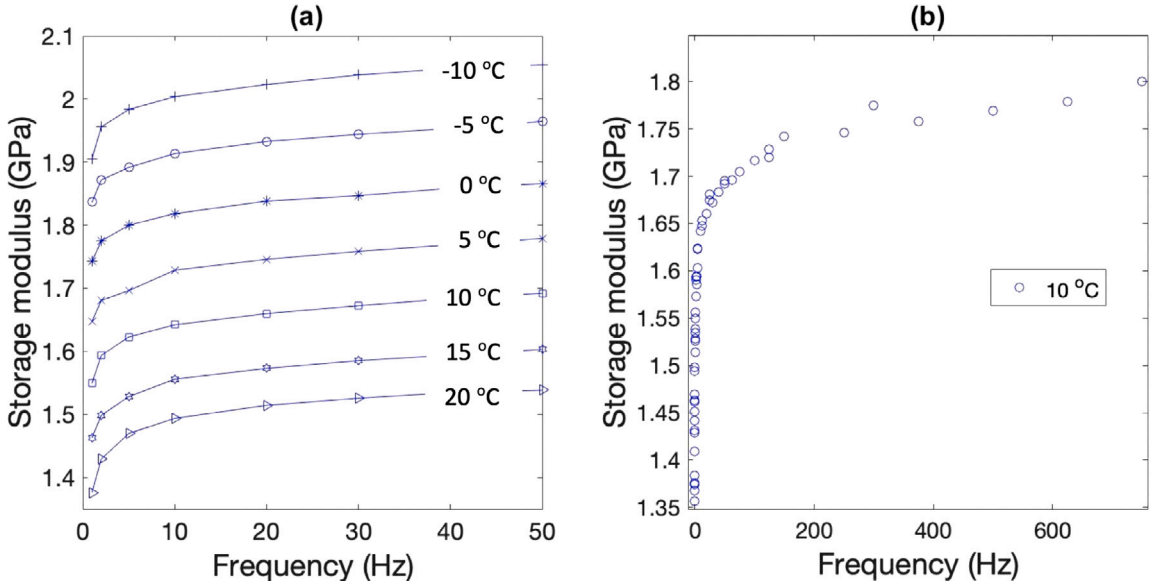

Fig. 8. (a) The storage modulus of a HDPE pipe sample as a function of frequency for various temperatures obtained with dynamic mechanical analysis. (b) The storage modulus of a HDPE pipe sample as a function of frequency after the application of time–temperature superposition for the reference temperature of 10 °C.

modulus predicted via the time–temperature superposition for the reference temperature of 10 °C. The storage modulus rises rapidly from its DC value to stabilize between 1.7 and 1.8 GPa at frequencies higher than 50 Hz. Compared to the values estimated via the vibro-acoustic method (see Fig. 7), the DMA results predict the storage modulus that is 0.4–0.5 GPa lower than that obtained via the vibro-acoustic method.

DMA was also applied on two PVC samples, sample P-1 (44 years old) and sample P-2 (3 years old). Fig. 9 depicts the DMA data after the application of time–temperature superposition. The deviation between the data of the PVC samples decreases as the frequency increases, from 22.2% at 10 Hz to 19% at 500 Hz. Additionally, if the uncertainty levels of the storage modulus of Set-up A are applied (Fig. 9(a)), there is a clear distinction between the estimated moduli. On the contrary, application of the uncertainty levels of Set-up B on the DMA data demonstrates that the overlap of the confidence intervals is so wide that they include both datasets (Fig. 9(b)).

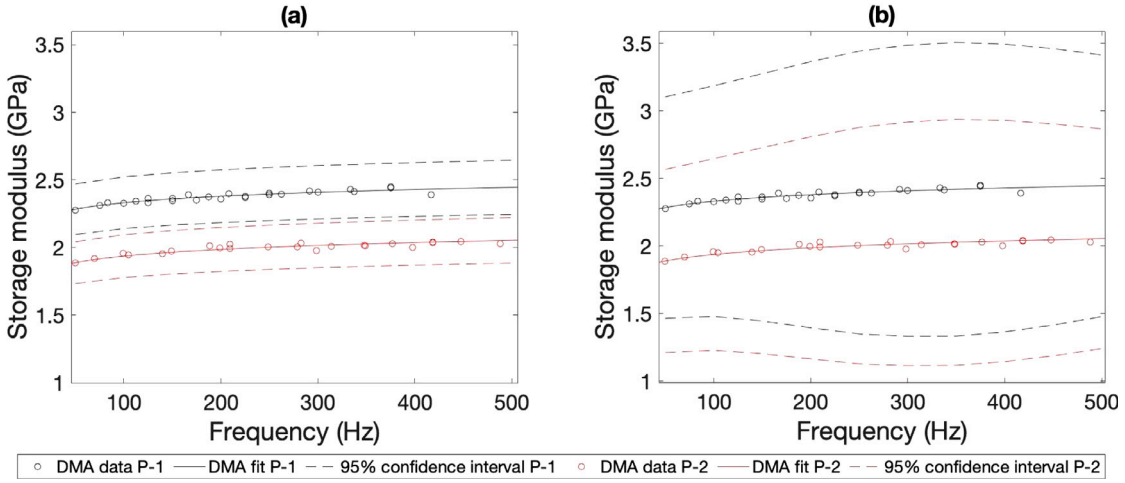

Fig. 9. The storage modulus of two pipe samples, sample P-1 (44 years old) and sample P-2 (3 years old), as a function of frequency after the application of time–temperature superposition on data obtained by dynamic mechanical analysis. The confidence intervals are the uncertainties in the acoustically estimated storage modulus for Set-up A (a) and Set-up B (b).

4. Discussion

An impact hammer and one or two hydrophones, depending on the set-up, proved to be sufficient in order to determine accurately the phase of the propagating fluid-borne wave and to use it subsequently to estimate the storage modulus. The use of an impact hammer facilitated accurate synchronization and guaranteed the excitation of a signal which includes only the impact response of the direct fluid-borne wave filtered out through the time windowing function (see Fig. 5). Other types of excitation (a shaker or a loudspeaker) would require to generate deterministic noise in a relatively broad frequency range and over a relatively long time span [28]. These signals can be more difficult to analyse in a pipe of a finite length because of the presence of multiple reflections from the pipe ends. It can be more difficult to estimate the optimal distance between the excitation source and receivers or distance between the receivers when these types of signals are adopted. The impact is rather difficult to estimate. Furthermore, successful application of vibro-acoustics to detect physical ageing of plastic pipes relies on two assumptions: (i) vibro-acoustics can be used to estimate the storage modulus of a plastic pipe, and (ii) the frequency-dependent storage modulus is sensitive to pipe ageing. Applications of this method are also affected by the measurement uncertainty. In this section the uncertainty is discussed based on the findings from the conducted experiments and analyses.

A comparison between the results from the DMA and vibro-acoustic experiments shows a systematic difference in the storage modulus of up to 0.5 GPa. This discrepancy could be attributed to a series of causes. Initially, the theory of acoustic waves was developed based on the conditions that all the elements of the system were isotropic and homogeneous, while the contact at the interface pipe–soil was assumed to be full and continuous. The above assumptions were necessary in order to produce a simpler and solvable system of equations. Nonetheless, it has to be realized that meeting these assumptions in practice would be very unlikely even in controlled laboratory conditions. Furthermore, depending on the method of measurement different estimates of the storage modulus can be obtained. For instance, when sample P-1 was subjected to conventional tensile tests, flexural tests and DMA, the value of elastic modulus was 3.09, 3.33 and 2.3–2.45 GPa (within 50–500 Hz), respectively [3]. Consequently, it is crucial that the same technique is applied consistently in order to draw consistent conclusions concerning changes in the pipe condition (e.g. ageing and stiffness). For the tested HDPE pipe samples, the value of the storage modulus estimated via vibro-acoustics (~2.2 GPa) was close to that quoted for HDPE pipes by Gao et al. (2 GPa) [29].

The DMA results for the two PVC pipe samples with an age difference of 41 years demonstrated a clear deviation in terms of measured storage modulus. The older sample showed a higher value of the storage modulus due to a lower ductility [1,3]. The observed deviation in the storage modulus decreased with increased frequency, a pattern that follows the findings in literature concerning the difficulty of ageing detection at higher frequencies [7,8]. However, estimating the storage modulus vibro-acoustically via the fluid-borne mode involves a higher uncertainty originating from individual uncertainties in the parameters in each medium of which the system consists. This affects the capability of the method to track ageing accurately. Results in this study showed that it is challenging to distinguish between different storage modulus values for the configuration when the pipe was surrounded by sand (Fig. 9(b)). Nonetheless, the considered uncertainty is not affected only by the addition of new parameters due to the presence of soil and their respective uncertainties. There is also a difference in the distance dz between the points at which the signals were recorded (5.3 m between the hammer and the single hydrophone in the above-ground section (Set-up A) and 0.3 m between the two hydrophones in the below-ground section (Set-up B)).

In order to analyse how the combined uncertainty in the storage modulus is formed, Eq. (3) was applied to estimate the individual parameter uncertainties. A normalization was applied with respect to the maximum uncertainty contribution at each considered

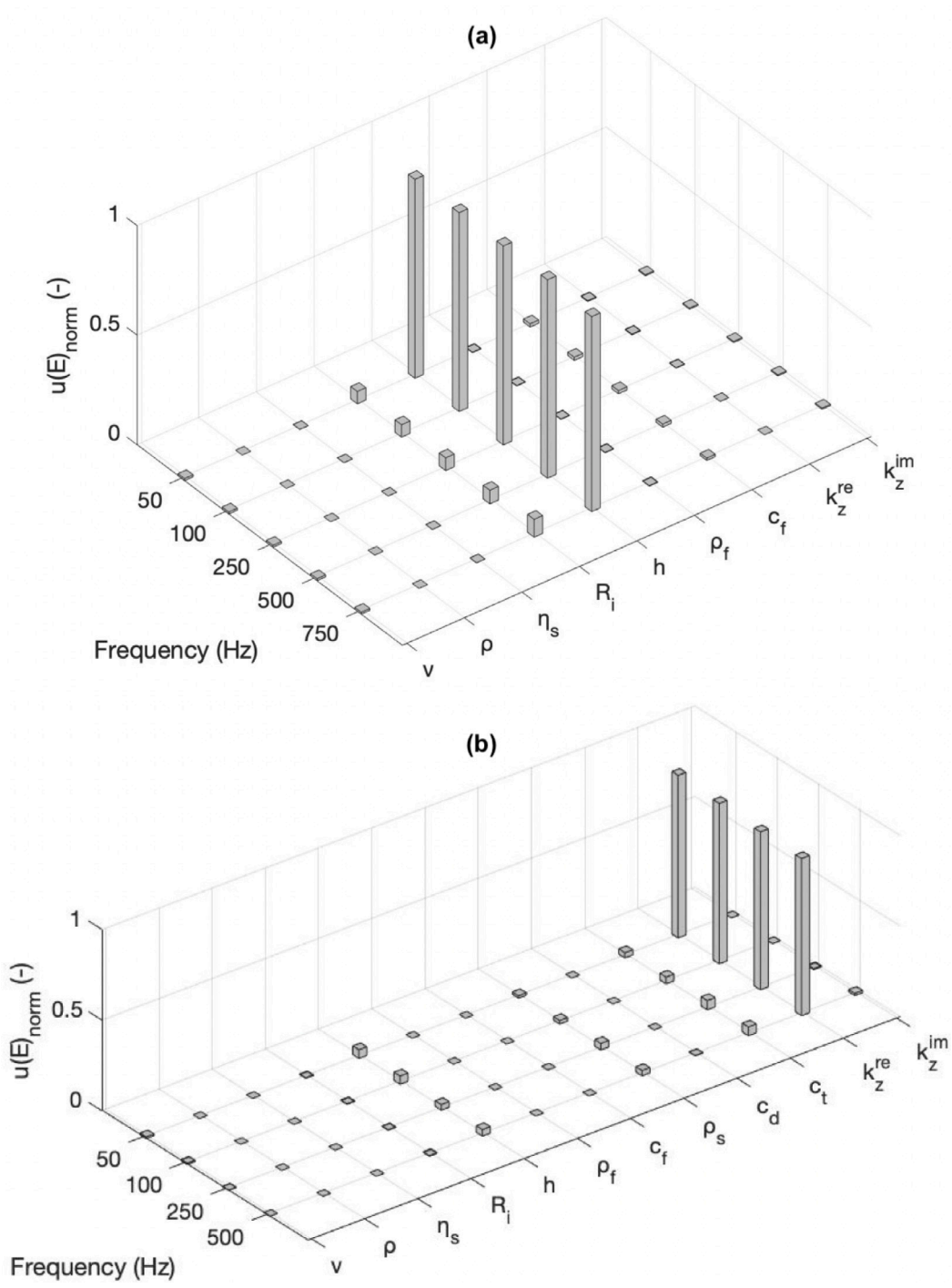

Fig. 10. The relative contribution of each parameter's uncertainty to the overall uncertainty of the pipe storage modulus $u(E)$ estimated via the axisymmetric fluid-borne wave for: Set-up A (a) and Set-up B (b). $u_{(E)}$ is normalized according to Eq. (5). (υ: pipe's Poisson ratio, ρ: pipe density, η_s: pipe loss factor, R_i: pipe internal radius, h: pipe wall thickness, ρ_f: fluid density, c_f: fluid sound velocity, ρ_s: soil density, c_d: soil compressional velocity, c_t: soil shear velocity, k_z^{re}: real axial wavenumber, k_z^{im}: imaginary axial wavenumber).

frequency. The normalized uncertainty of the storage modulus $u(E)_{norm}$ for every parameter x_i was defined as:

$$u(E)_{norm} = \frac{u(E)_{x_i}}{max(u(E)_{x_i}, \ldots, u(E)_{x_N})} \quad (5)$$

where $u(E)_{x_i}$ is the uncertainty in the storage modulus caused by the individual uncertainty of parameter x_i at a given frequency.

Fig. 10 presents the normalized relative contribution of each parameter's uncertainty to the overall uncertainty of the storage modulus estimation for Set-up A (Fig. 10(a)) and Set-up B (Fig. 10(b)). In the case of Set-up A the derived uncertainty in the storage modulus (Fig. 7(a)) originates mostly from a lack of accurate data on the pipe geometry, especially the pipe wall thickness. In the considered frequency range (50–750 Hz), the relative contribution of the uncertainty in the pipe wall thickness and internal radius to the overall uncertainty is ~90% and 6%–8%, respectively. It should be noted that if the uncertainty in the wall thickness and internal radius decreases from 0.5 to 0.1 mm, then the overall uncertainty in the estimation of the pipe's storage modulus drops from ~0.2 to ~0.04 GPa, a characteristic that would allow the proposed method to become significantly more sensitive to the modulus changes due to ageing. The rest of the parameters have a minor effect.

In the case of Set-up B, most of the overall uncertainty (~90%) is attributed to the uncertainty in the real part of the axial wavenumber ($u(k_z^{re})$). Eq. (4) reveals the factors that contribute to an increase in the uncertainty of k_z^{re}. The distance between the hydrophones is an influencing parameter as it is in both denominators while being raised in the power of 2 and 4. Therefore, values of dz lower than unity are expected to increase $u(k_z^{re})$, whereas values larger than unity would have the opposite effect. It should be stressed that Eq. (4) applies irrespectively of the surrounding conditions (in vacuum or soil), and the type of excitation or signal reception sensors. The effect of distance is reflected in the width of confidence intervals of k_z^{re} in Fig. 6 for the considered values of 5.3 in Set-up A and 0.3 m in Set-up B (Figs. 6(a) and 6(b), respectively). Additionally, in the case of Set-up B a higher uncertainty in the phase difference $d\phi$ was predicted, although there is not a clear proof regarding the origin of it. Possible reasons can include inconsistent coupling at the pipe–sand interface, elastomeric joint and/or transition from a fully covered by soil pipe section to a section surrounded only by air required to provide easy access to the two hydrophones (see Fig. 1(c)).

This study assumed considerably higher uncertainties in the soil parameters compared to those quoted for the pipe material and water (Table 1). However, the results presented in Fig. 10(b) suggest that the contribution to the overall uncertainty from the uncertainties in the soil parameters is similar to or less than that from the uncertainty in the pipe wall thickness (~5%). Therefore, a lack of accurate knowledge of the parameters of surrounding soil is unlikely to hinder the applicability of the presented vibro-acoustic method, although a lower uncertainty of the soil's shear wave velocity and density at specific frequencies would be beneficial. The effect of the soil's shear velocity on the fluid-borne mode is also shown in the literature [28,30]. Finally, the assumption that the imaginary part of the axial wavenumber (k_z^{re}) was zero proved to have minimal effect on the overall uncertainty in the estimated storage modulus. It should be stressed that applying such a condition requires that the values of $u(k_z^{im})$ are similar to the magnitude of the expected true values of k_z^{im} at each considered frequency.

5. Conclusions

This study explored the use of the vibro-acoustic axisymmetric fluid-borne mode to estimate the storage modulus of two high-density polyethylene pipes and to relate it to ageing. This was based on the measurement of the real part of the modal wavenumber in a pipe surrounded by air and a pipe buried in sand. The both experimental configurations (above and below ground) proved to be capable of identifying similar values for the pipe's storage modulus (~ 2.2 GPa). A 0.4–0.5 GPa higher value of the storage modulus was obtained via acoustic data compared to the results from dynamic mechanical analysis (DMA).

DMA on samples from two PVC pipes with 41 years extrusion age difference revealed that ageing can be detected via the storage modulus estimated from vibro-acoustic data at low frequencies (<500 Hz). The proposed vibro-acoustic method yields results with an overall uncertainty that depends on a combination of uncertainties in the parameters of the embedded media (pipe, water, soil). A larger distance between the locations of the two receiving signals results in a lower overall uncertainty in the real part of the modal wavenumber. The accurate knowledge of the pipe's geometry (wall thickness and internal radius) is paramount, as it is a key parameter that contributes to the overall uncertainty. Especially the uncertainty in the pipe wall thickness affects significantly the overall uncertainty. The presence or absence of soil around the pipe has a relatively small effect in comparison with the uncertainty in the wall thickness. However, a better knowledge of the true shear wave velocity in soil and soil density would be beneficial to reduce the overall uncertainty. The uncertainty analysis suggests that the knowledge of the imaginary part of the axial wavenumber is unimportant to estimate the pipe's storage modulus and associated uncertainties.

CRediT authorship contribution statement

Konstantinos F. Makris: Experimental work (vibro-acoustics), Formal analysis, Visualization, Writing – original draft. **Jeroen G. Langeveld:** Supervision, Writing – review & editing. **François H.L.R. Clemens-Meyer:** Supervision, Writing – review & editing. **Joanna Watts:** Experimental work (vibro-acoustics). **Hasina Begum:** Experimental work (DMA). **Kirill V. Horoshenkov:** Supervision, Advice on data analysis, Writing – review & editing.

Data availability

Data will be made available on request.

Acknowledgements

This research is conducted under the "Kennisprogramma Urban Drainage" (Knowledge Programme Urban Drainage). The involved parties are: ARCADIS, Deltares, Gemeente Almere, Gemeente Breda, Gemeente's-Gravenhage, Gemeentewerken Rotterdam, Gemeente Utrecht, GMB Rioleringstechniek, KWR Watercycle Research Institute, Platform Water Vallei en Eem, Royal HaskoningDHV, Stichting RIONED, STOWA, Sweco Nederland, Tauw, vandervalk+degroot, Waterboard De Dommel, Waternet and Witteveen+Bos. This research was also supported by UK Engineering and Physical Sciences Research Council (EPSRC), Grant EP/S016813/1. The authors are grateful to Professor Simon Tait and Dr. Will Shepherd for granting the access to the pipe facility at the Sheffield's Integrated Civil and Infrastructure Research Centre (www.icair.ac.uk). The authors are also grateful to the technical staff at the University of Sheffield, Mrs. Paul Osborne and Mr. Mathew Hall, for their help with the experiments. For the purpose of open access, the author has applied a 'Creative Commons Attribution (CC BY) licence to any Author Accepted Manuscript version arising'.

Appendix A. Derivation of the dispersion equations

This section includes the derivation of the dispersion equation for a fluid-filled pipe surrounded by soil, hereafter called "fluid–pipe–soil" system. The general equation is reduced for the case of axisymmetric modes and for a fluid-filled pipe in vacuum, hereafter called "fluid–pipe–vacuum" system. The solution of the "fluid–pipe–vacuum" system can be used for pipes surrounded by air under the assumption that the effect of air on wave propagation is negligible. Fig. A.1 presents the applied coordinate system and the notation of the displacement fields used for this analysis.

A.1. Pipe shell domain

The equations of motion for the pipe shell can be written in the matrix form [31]:

$$[Q][u_j] = 0 \tag{A.1}$$

where $[Q]$ is a matrix differential operator, and u_j is the displacement (j=z, θ, r).

Eq. (A.1) could be reformed with respect to the displacement amplitudes (U_j), if general wave solutions are assumed for the pipe displacement components:

$$[u_j] = [U_j]e^{in\theta}e^{i(\omega t - k_z z)} \tag{A.2}$$

where U_j is the shell displacement amplitude for $j = z$, θ and r, n is the circumferential order (=0 for axisymmetric modes), ω is the angular frequency, k_z is the axial wavenumber, and $i = \sqrt{-1}$.

Various theories describing the motion of thin cylindrical shells have been established. Depending on the adopted shell theory, a different operator $[Q]$ has been proposed. According to the Donnel–Mushtari theory, the operator Q used for this analysis, after considering Eq. (A.2), is [31]:

$$Q = \begin{bmatrix} \Omega^2 - k_z^2 R^2 - n^2 \frac{(1-\upsilon)}{2} & k_z R n \frac{(1+\upsilon)}{2} & -k_z R \upsilon i \\ k_z R n \frac{(1+\upsilon)}{2} & \Omega^2 - k_z^2 R^2 \frac{(1-\upsilon)}{2} - n^2 & n i \\ -k_z R \upsilon i & n i & -\Omega^2 + 1 + \beta^2 (n^2 + k_z^2 R^2)^2 \end{bmatrix} \tag{A.3}$$

where υ is the Poisson ratio, R is the mean radius, $\beta^2 = h^2/12R^2$ (h being the wall thickness), and $\Omega = \omega R\sqrt{\rho(1-\upsilon^2)/E}$, ρ is the density of the pipe material, E is the complex modulus ($E = E'(1 + \eta_s i)$, E' being the storage modulus and η_s the loss factor).

A.2. Soil domain

Assuming a homogeneous, isotropic and linear elastic soil medium, the equation of motion in the soil domain can be expressed via the Navier's governing wave equation [32]:

$$(\mu_s + \lambda_s)\nabla(\nabla \cdot \vec{V}) + \mu_s \nabla^2 \vec{V} = \rho_s \frac{\partial^2 \vec{V}}{\partial t^2} \tag{A.4}$$

where $\vec{V}$ is the soil displacement vector, μ_s and λ_s are the Lamé constants, ρ_s is the soil density, $\nabla \cdot \vec{V}$ is the divergence of $\vec{V}$, ∇ is the gradient, and ∇^2 is the Laplace operator.

Moreover, the soil displacement components can be expressed by means of three potential functions Φ, X, Ψ [33]:

$$\upsilon_z = \frac{\partial \Phi}{\partial z} - \frac{1}{r}\frac{\partial (r \frac{\partial X}{\partial r})}{\partial r} - \frac{1}{r^2}\frac{\partial^2 X}{\partial \theta^2} \tag{A.5a}$$

$$\upsilon_\theta = \frac{1}{r}\frac{\partial \Phi}{\partial \theta} - \frac{\partial \Psi}{\partial r} + \frac{1}{r}\frac{\partial^2 X}{\partial z \partial \theta} \tag{A.5b}$$

$$\upsilon_r = \frac{\partial \Phi}{\partial r} + \frac{1}{r}\frac{\partial \Psi}{\partial \theta} + \frac{\partial^2 X}{\partial z \partial r} \tag{A.5c}$$

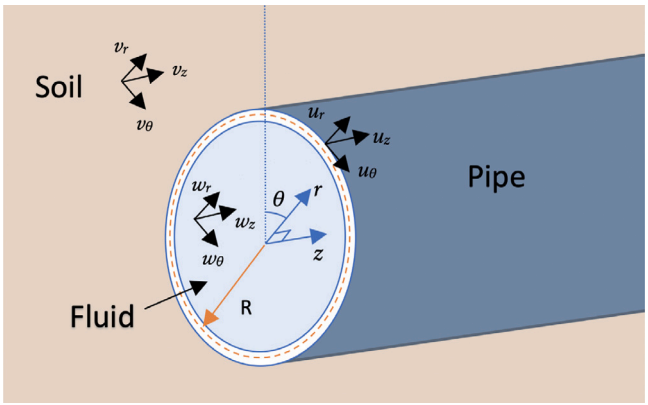

Fig. A.1. A sketch of a water–pipe–soil coupled system and cylindrical system of coordinates. The vectors u, v and w correspond to the displacements in the pipe, soil and fluid propagation media respectively, and the subscripts (z, θ, r) correspond to the respective directions.

The equation of motion (Eq. (A.4)) is satisfied if the potential functions satisfy the following three uncoupled equations for wave propagation:

$$\nabla^2 \boldsymbol{\Phi} = \frac{1}{c_d^2} \frac{\partial^2 \boldsymbol{\Phi}}{\partial t^2} \tag{A.6a}$$

$$\nabla^2 X = \frac{1}{c_\tau^2} \frac{\partial^2 X}{\partial t^2} \tag{A.6b}$$

$$\nabla^2 \boldsymbol{\Psi} = \frac{1}{c_\tau^2} \frac{\partial^2 \boldsymbol{\Psi}}{\partial t^2} \tag{A.6c}$$

where c_d and c_t are the soil compressional and shear wave propagation velocities, respectively:

$$c_d = \sqrt{\frac{2\mu_s + \lambda_s}{\rho_s}} \tag{A.7a}$$

$$c_\tau = \sqrt{\frac{\mu_s}{\rho_s}} \tag{A.7b}$$

Furthermore, the solutions of Eq. (A.6) can be expressed via the Hankel functions of the second kind so that the potential functions approach 0 as $r \to \infty$ [34]:

$$\boldsymbol{\Phi} = A\, H_n(k_{d,r} r)\, e^{(in\theta)}\, e^{(i(\omega t - k_z z))} \tag{A.8a}$$

$$\boldsymbol{\Psi} = B\, H_n(k_{\tau,r} r)\, e^{(in\theta)}\, e^{(i(\omega t - k_z z))} \tag{A.8b}$$

$$X = C\, H_n(k_{\tau,r} r)\, e^{(in\theta)}\, e^{(i(\omega t - k_z z))} \tag{A.8c}$$

where A, B and C are constant coefficients, and H_n is the Hankel function of the second kind of order n. The terms $k_{d,r}$ and $k_{\tau,r}$ are radial wavenumbers related to the compressional (k_d) and shear (k_τ) wavenumbers via the relationships:

$$k_{d,r} = \sqrt{k_d^2 - k_z^2} \tag{A.9a}$$

$$k_{\tau,r} = \sqrt{k_\tau^2 - k_z^2} \tag{A.9b}$$

Substitution of Eq. (A.8) into Eq. (A.5) leads to functions of the soil displacement components with respect to the coefficients A, B and C:

$$\begin{bmatrix} v_z \\ v_\theta \\ v_r \end{bmatrix} = \begin{bmatrix} K_{11} & K_{12} & K_{13} \\ K_{21} & K_{22} & K_{23} \\ K_{31} & K_{32} & K_{33} \end{bmatrix} \begin{bmatrix} A \\ B \\ C \end{bmatrix} e^{in\theta}\, e^{i(\omega t - k_z z)} \tag{A.10}$$

where

$$K_{11} = -k_z\, H_n(k_d^r\, r)\, i$$
$$K_{12} = 0$$
$$K_{13} = -\frac{1}{r}\, k_\tau^r\, H_n'(k_\tau^r\, r) - (k_\tau^r)^2\, H_n''(k_\tau^r\, r) + \frac{1}{r^2}\, n^2\, H_n(k_\tau^r\, r)$$
$$K_{21} = \frac{1}{r}\, n\, H_n(k_d^r\, r)\, i$$
$$K_{22} = -k_\tau^r\, H_n'(k_\tau^r\, r)$$
$$K_{23} = \frac{1}{r}\, k_z\, n\, H_n(k_\tau^r\, r)$$
$$K_{31} = k_d^r\, H_n'(k_d^r\, r)$$
$$K_{32} = \frac{1}{r}\, n\, H_n(k_\tau^r\, r)\, i$$
$$K_{33} = -k_z\, k_\tau^r\, H_n'(k_\tau^r\, r)\, i$$

Furthermore, the stress–strain relationships based on the Hooke's law for an isotropic medium are given by:

$$\begin{aligned} \sigma_{rr} &= (\lambda_s + 2\mu_s)\, \epsilon_{rr} + \lambda_s\, \epsilon_{\theta\theta} + \lambda_s\, \epsilon_{zz} = \lambda_s\, \nabla^2 \Phi + 2\mu_s\, \epsilon_{rr} \\ \sigma_{r\theta} &= \mu_s\, \gamma_{r\theta} \\ \sigma_{rz} &= \mu_s\, \gamma_{rz} \end{aligned} \tag{A.11}$$

where the strains are expressed via the soil displacement components through the relationships:

$$\begin{aligned} \epsilon_{rr} &= \frac{\partial v_r}{\partial r} \\ \epsilon_{zz} &= \frac{\partial v_z}{\partial z} \\ \epsilon_{\theta\theta} &= \frac{v_r}{r} + \frac{1}{r}\, \frac{\partial v_\theta}{\partial \theta} \\ \gamma_{r\theta} &= \frac{\partial v_\theta}{\partial r} + \frac{1}{r}\, \frac{\partial v_r}{\partial \theta} - \frac{v_\theta}{r} \\ \gamma_{rz} &= \frac{\partial v_z}{\partial r} + \frac{\partial v_r}{\partial z} \end{aligned} \tag{A.12}$$

Consequently, the stresses can be expressed via the coefficients A, B and C:

$$\begin{bmatrix} \sigma_{rz} \\ \sigma_{r\theta} \\ \sigma_{rr} \end{bmatrix} = \begin{bmatrix} L_{11} & L_{12} & L_{13} \\ L_{21} & L_{22} & L_{23} \\ L_{31} & L_{32} & L_{33} \end{bmatrix} \begin{bmatrix} A \\ B \\ C \end{bmatrix} e^{in\theta}\, e^{i(\omega t - k_z z)} \tag{A.13}$$

where

$$L_{11} = -2\mu_s\, k_z\, k_d^r\, H_n'(k_d^r\, r)\, i$$
$$L_{12} = \mu_s\, \frac{1}{r}\, k_z\, n\, H_n(k_\tau^r\, r)$$
$$L_{13} = -\mu_s\, (k_z^2\, k_\tau^r\, H_n'(k_\tau^r\, r) + \frac{1}{r}\, (k_\tau^r)^2\, H_n''(k_\tau^r\, r) - \frac{1}{r^2}\, k_\tau^r\, H_n'(k_\tau^r\, r) + (k_\tau^r)^3\, H_n'''(k_\tau^r\, r) - \frac{1}{r^2}\, n^2\, k_\tau^r\, H_n'(k_\tau^r\, r) + \frac{2}{r^3}\, n^2\, H_n(k_\tau^r\, r))$$
$$L_{21} = \mu_s\, (\frac{2}{r}\, n\, k_d^r\, H_n'(k_d^r\, r) - \frac{2}{r^2}\, n\, H_n(k_d^r\, r))\, i$$
$$L_{22} = \mu_s\, (\frac{1}{r}\, k_\tau^r\, H_n'(k_\tau^r\, r) - \frac{1}{r^2}\, n^2\, H_n(k_\tau^r\, r) - (k_\tau^r)^2\, H_n''(k_\tau^r\, r))\, i$$
$$L_{23} = \mu_s\, (\frac{2}{r}\, k_z\, n\, k_\tau^r\, H_n'(k_\tau^r\, r) - \frac{2}{r^2}\, k_z\, n\, H_n(k_\tau^r\, r))\, i$$
$$L_{31} = (\lambda_s + 2\mu_s)\, ((k_d^r)^2\, H_n''(k_d^r\, r)) + \lambda_s\, (\frac{1}{r}\, k_d^r\, H_n'(k_d^r\, r) - \frac{1}{r^2}\, n^2\, H_n(k_d^r\, r) - k_z^2\, H_n(k_d^r\, r))$$
$$L_{32} = 2\mu_s\, (\frac{1}{r}\, n\, k_\tau^r\, H_n'(k_\tau^r\, r) - \frac{1}{r^2}\, n\, H_n(k_\tau^r\, r))\, i$$
$$L_{33} = -2\mu_s\, k_z\, (k_\tau^r)^2\, H_n''(k_\tau^r\, r)\, i$$

A.3. Fluid domain

Fig. A.2 illustrates a fluid element excited by the sound pressure wave. By applying the Newton's second law with respect to the r direction, the following relationship between the pressure and displacement is obtained [34]:

$$(P_s + p)\, S - (P_s + p + \frac{\partial p}{\partial r} dr)\, S = \rho_f\, \frac{\partial^2 w_r}{\partial t^2}\, S\, dr$$

$$\frac{\partial p}{\partial r} = -\rho_f\, \frac{\partial^2 w_r}{\partial t^2} \tag{A.14}$$

where S is the cross-section of the fluid element perpendicular to the r direction and ρ_f is the fluid density, P_s is the static pressure, p is the acoustic pressure, and w_r is the displacement of the fluid in the r direction.

Further, the pressure field is expected to be in the form of modal series with a radial configuration expressed via Bessel functions of the first kind [34,35]. Assuming axial travelling waves, the pressure field in the fluid can be represented as:

$$p_{in} = P_{in}\, J_n(K_{f,r}\, r)\, e^{in\theta}\, e^{i(\omega t - k_z z)} \tag{A.15}$$

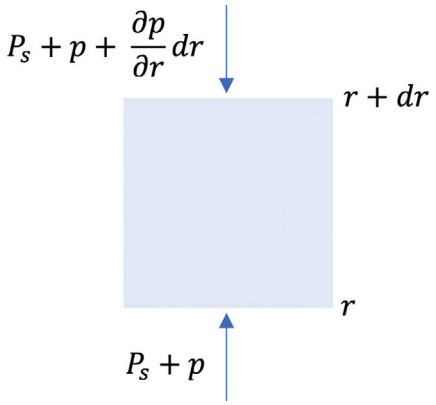

Fig. A.2. Pressure components acting on a fluid element in the r direction.

where P_{in} is the pressure amplitude, J_n is the Bessel function of the first kind and order n, and $k_{f,r}$ is the fluid radial wavenumber given by $k_{f,r} = \sqrt{k_f^2 - k_z^2}$.

A.4. Coupling at the pipe–soil interface

The coupling between the pipe and soil is performed under the assumption of absolute contact, which implies that the following boundary conditions are applied at the pipe–soil interface:

$$u_i = v_i, \qquad i = z, \theta, r \tag{A.16}$$

Substituting Eq. (A.2) and Eq. (A.10) into Eq. (A.16), and rearranging terms leads to:

$$\begin{bmatrix} A \\ B \\ C \end{bmatrix} = \begin{bmatrix} U_z \\ U_\theta \\ U_r \end{bmatrix} \begin{bmatrix} K_{11} & K_{12} & K_{13} \\ K_{21} & K_{22} & K_{23} \\ K_{31} & K_{32} & K_{33} \end{bmatrix}^{-1} \tag{A.17}$$

Hence, the pressure exerted from the pipe shell towards soil can be written with the aid of Eq. (A.13) in the following form:

$$\begin{bmatrix} \sigma_{rz} \\ \sigma_{r\theta} \\ \sigma_{rr} \end{bmatrix} = \begin{bmatrix} L_{11} & L_{12} & L_{13} \\ L_{21} & L_{22} & L_{23} \\ L_{31} & L_{32} & L_{33} \end{bmatrix} \begin{bmatrix} K_{11} & K_{12} & K_{13} \\ K_{21} & K_{22} & K_{23} \\ K_{31} & K_{32} & K_{33} \end{bmatrix}^{-1} \begin{bmatrix} U_z \\ U_\theta \\ U_r \end{bmatrix} e^{in\theta}\, e^{i(\omega t - k_z z)} \tag{A.18}$$

A.5. Coupling at the fluid–pipe interface

Similar conditions are assumed to apply at the pipe–fluid interface (i.e. perfect contact):

$$u_i = w_i, \qquad i = z, \theta, r \tag{A.19}$$

This method is developed by regarding water as the internal fluid medium, which is considered to be inviscid. Hence, it cannot sustain shear stresses and substitution of Eq. (A.2) in the r direction and Eq. (A.15) into Eq. (A.14) leads to a relationship between the pressure amplitude P_{in} and the displacement amplitude in water W_r:

$$P_{in} = \frac{\rho_f\, \omega^2}{k_{f,r}\, J_n'(k_{f,r}\, r)}\, W_r \tag{A.20}$$

Therefore, Eq. (A.15) is expressed with respect to the shell amplitude U_r based on Eq. (A.19):

$$p_{in} = U_r\, P\, e^{in\theta}\, e^{i(\omega t - k_z z)} \tag{A.21}$$

where

$$P = \frac{\rho_f \omega^2 J_n(k_{f,r} r)}{k_{f,r} J_n'(k_{f,r} r)}. \tag{A.22}$$

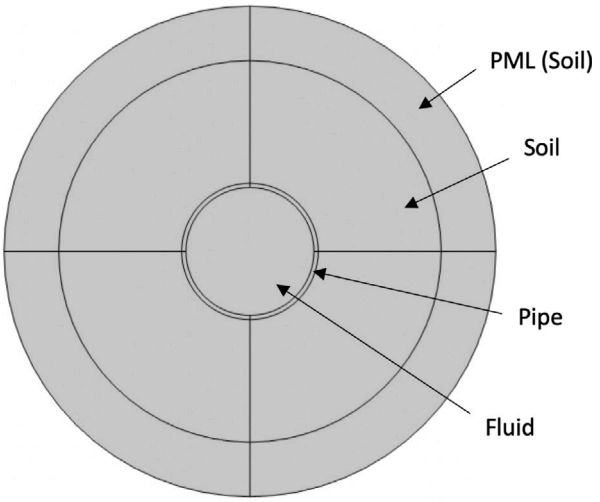

Fig. B.1. Geometry of the COMSOL® model used for deriving the dispersion curves of a water-filled pipe surrounded by soil.

A.6. General solution

The complete equations of motion can be expressed via the displacement amplitudes U_z, U_θ and U_r, by considering Eqs. (A.18) and (A.21):

$$\left\{[Q]+\frac{(1-v^2)\,R^2}{E\,h}\left(\begin{bmatrix}L_{11}&L_{12}&L_{13}\\L_{21}&L_{22}&L_{23}\\-L_{31}&-L_{32}&-L_{33}\end{bmatrix}\begin{bmatrix}K_{11}&K_{12}&K_{13}\\K_{21}&K_{22}&K_{23}\\K_{31}&K_{32}&K_{33}\end{bmatrix}^{-1}+P\begin{bmatrix}0&0&0\\0&0&0\\0&0&-1\end{bmatrix}\right)\right\}\begin{bmatrix}U_z\\U_\theta\\U_r\end{bmatrix}=0 \tag{A.23}$$

Non-trivial solutions of Eq. (A.22) exist only if the determinant of the coefficients is equal to zero. These solutions define the characteristic dispersion equation of the studied system. For measured axial wavenumbers, the solution for the storage modulus of the pipe material can be found. Solutions can be obtained for the system "fluid–pipe–vacuum" by setting $L_{ij}=K_{ij}=0\ (i,j=1,2,3)$.

A.7. Axisymmetric wave propagation

In axisymmetric wave propagation, the displacement field is independent of the circumferential angle (n=0). Eq. (A.22) can be further simplified by neglecting the dependence of the displacements on the θ direction. Subsequently, the solutions can be traced by setting:

$$det\left\{[Q]+\frac{(1-v^2)\,R^2}{E\,h}\left(\begin{bmatrix}L_{11}&L_{13}\\-L_{31}&-L_{33}\end{bmatrix}\begin{bmatrix}K_{11}&K_{13}\\K_{31}&K_{33}\end{bmatrix}^{-1}+P\begin{bmatrix}0&0\\0&-1\end{bmatrix}\right)\right\}_{n=0}=0 \tag{A.24}$$

Appendix B. Dispersion curves from numerical analysis

B.1. Theoretical background

This section presents the theory behind the development of a 2D finite element model (FEM) in COMSOL Multiphysics® for deriving dispersion curves of a fluid-filled pipe in vacuum or surrounded by soil (Fig. B.1). The 2D model represents a cross-section of the system characterized by harmonic modes in space and uniform extension in the out-of-plane direction [36]. Solutions of the out-of-plane wavenumber for a given frequency are obtained via the modal analysis with a built-in frequency domain eigensolver. Therefore, all the given equations in this section are considered in the frequency domain.

Within the fluid domain, the solutions for the out-of-plane wavenumber k_z are sought by solving the Helmholtz equation:

$$\nabla\left(-\frac{1}{\rho_f}\nabla p\right)-\frac{k_{f,r}^2\,p}{\rho_f}=0 \tag{B.1}$$

where $k_{f,r}^2=(\frac{\omega}{c_f})^2-k_z^2$, p is the acoustic pressure, ρ_f is the fluid density, and c_f is the fluid sound velocity.

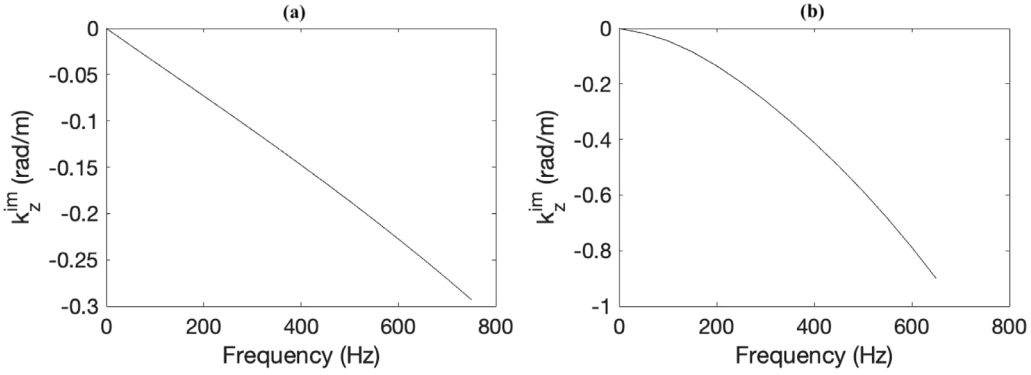

Fig. B.2. Imaginary parts of the axial wavenumber solutions in COMSOL® for Set-up A (a) and Set-up B (b).

Within the pipe and soil domain, the solutions for k_z are found by assuming linear elasticity and that $u(x, y, z) = u(x, y)\, e^{-k_z z}$, where x, y, z are the cartesian space coordinates:

$$-\rho\, \omega^2\, \vec{u} = \nabla\, S \tag{B.2}$$

where ρ is the density of the medium, $\vec{u}$ is the solid displacement vector, $S = C_{jk}\, \epsilon_{jk}$ (C_{jk} being the elasticity tensor and ϵ_{jk} the elastic strain for $j, k = x, y, z$).

The coupling at the acoustic–structure interface is implemented by applying the following conditions on the inner and outer boundary of the interface [37]:

$$\begin{aligned} -\vec{n}(-\frac{1}{\rho_f}\nabla p) &= -\vec{n}\,\frac{\partial^2 \vec{u}}{\partial t^2} \\ \overrightarrow{F_A} &= p\,\vec{n} \end{aligned} \tag{B.3}$$

where $\vec{n}$ is the surface normal, and $\overrightarrow{F_A}$ is the load applied on the pipe.

In case the pipe is surrounded by soil, a Perfectly Matched Layer (PML) is applied at the external edge of the soil domain in order to model the infinite extents of the system. PML is used in order to dissipate the propagating waves with minimal reflections back to the system. This is achieved by applying a polynomial stretching function within the PML [37]:

$$f_p(\xi) = s\, \xi^c\, (1 - i) \tag{B.4}$$

where ξ is a dimensionless coordinate (from 0 to 1) which extents along the PML, s is the scaling factor, c is the curvature parameter, and $i = \sqrt{-1}$. In this study, the default values (= 1) were used for both scaling factor and curvature parameter without further tuning.

B.2. Input for uncertainty analysis

The imaginary part of the axial wavenumber could not be extracted from the conducted vibro-acoustic experiments. Consequently, the imaginary part of the axial wavenumber was assumed to be zero at all frequencies and the respective uncertainty was considered to be the expected value of imaginary wavenumber. The latter was given by solving a finite element COMSOL® model. The pipe shell, water and soil properties are given in Table 1. Further, the storage modulus of the pipe shell used as input in both models was obtained by the results of the dynamic mechanical analysis (Fig. 8b). Fig. B.2 demonstrates the imaginary parts of the axial wavenumber for the fluid-borne mode concerning the two different set-ups utilized for this analysis (Set-up A and Set-up B).

References

[1] H.A. Visser, Residual lifetime assessment of uPVC gas pipes, (Doctoral Dissertation), University of Twente, Enschede, The Netherlands, 2009, http://dx.doi.org/10.3990/1.9789036529587.

[2] E. Drenth, Towards Condition Based Asset Management of UPVC Pipes, (Doctoral Dissertation), University of Twente, Enschede, The Netherlands, 2015, http://dx.doi.org/10.3990/1.9789036539920.

[3] K.F. Makris, J.G. Langeveld, F.H.L.R. Clemens, Extensive testing on PVC sewer pipes towards identifying the factors that affect their operational lifetime, Struct. Infrastruct. Eng. 18 (12) (2022) 1601–1613, http://dx.doi.org/10.1080/15732479.2021.1907601.

[4] L.C.E. Struik, Physical aging in amorphous polymers and other materials (Doctoral Dissertation) (Ph.D. thesis), Delft University of Technology, The Netherlands, 1977, Retrieved from http://resolver.tudelft.nl/uuid:941d2af6-903a-4260-9953-2efb4cb38d2e.

[5] L.A. Fillot, P. Hajji, C. Gauthier, K. Masenelli-Varlot, Thermomechanical history effects on rigid PVC microstructure and impact properties, J. Appl. Polym. Sci. 104 (2007) 2009–2017, http://dx.doi.org/10.1002/app.25688.

[6] R. Flores, J.Z. Pérez, P. Cassagnau, A. Michel, J.-Y. Cavaillé, α Mechanical relaxation in poly(vinyl chloride): effect of ageing and crosslinking, Polymer 35 (1994) 2800–2807, 10.1016/0032-3861(94)90309-3.

[7] B.E. Read, G.D. Dean, P.E. Tomlins, J.L. Lesniarek-Hamid, Physical ageing and creep in PVC, Polymer 33 (13) (1992) 2689–2698, http://dx.doi.org/10.1016/0032-3861(92)90439-4.
[8] A. Demčenko, Development and Analysis of Noncollinear Wave Mixing Techniques for Material Properties Evaluation using Immersion Ultrasonics, (Doctoral Dissertation), University of Twente, Enschede, The Netherlands, 2014, http://dx.doi.org/10.3990/1.9789036537612.
[9] H. Delgadillo, Ultrasonic Inspection of Drinking Water Mains, (Doctoral Dissertation), University of Twente, Enschede, The Netherlands, 2019, http://dx.doi.org/10.3990/1.9789036548533.
[10] D.G. Ivey, B.A. Mrowca, E. Guth, Propagation of ultrasonic bulk waves in high polymers, J. Appl. Phys. 20 (1949) 486–492, http://dx.doi.org/10.1063/1.1698415.
[11] S. Koda, K. Yamashita, K. Matsumoto, H. Nomura, Characterization of polyvinylchloride by means of sound velocity and longitudinal modulus measurements, Japan. J. Appl. Phys. 32 (1993) 2234–2237.
[12] K. Baik, J. Jiang, T.G. Leighton, Acoustic attenuation, phase and group velocities in liquid-filled pipes: Theory, experiment, and examples of water and mercury, J. Acoust. Soc. Am. 128 (5) (2010) 2610–2624, http://dx.doi.org/10.1121/1.3495943.
[13] R. Long, P. Cawley, M. Lowe, Acoustic wave propagation in buried iron water pipes, in: Proceedings of the Royal Society of London. Series a: Mathematical, Physical and Engineering Sciences, Vol. 459, (2039) 2003, pp. 2749–2770, http://dx.doi.org/10.1098/rspa.2003.1148.
[14] Y. Gao, M.J. Brennan, P.F. Joseph, J.M. Muggleton, O. Hunaidi, A model of the correlation function of leak noise in buried plastic pipes, J. Sound Vib. 277 (1-2) (2004) 133–148, http://dx.doi.org/10.1016/j.jsv.2003.08.045.
[15] O. Scussel, M.J. Brennan, F.C.L. Almeida, J. Muggleton, E. Rustighi, P.F. Joseph, Estimating the spectrum of leak noise in buried plastic water distribution pipes using acoustic or vibration measurements remote from the leak, Mech. Syst. Signal Process. 147 (2021) http://dx.doi.org/10.1016/j.ymssp.2020.107059.
[16] O. Scussel, M.J. Brennan, J.M. Muggleton, F.C.L. Almeida, A.T. Paschoalini, Estimation of the bulk and shear moduli of soil surrounding a plastic water pipe using measurements of the predominantly fluid wave in the pipe, J. Appl. Geophys. 164 (2019) 237–246, http://dx.doi.org/10.1016/j.jappgeo.2019.01.010.
[17] Y. Gao, J.M. Muggleton, Y. Liu, E. Rustighi, An analytical model of ground surface vibration due to axisymmetric wave motion in buried fluid-filled pipes, J. Sound Vib. 395 (2017) 142–159, http://dx.doi.org/10.1016/j.jsv.2017.02.022.
[18] R. Pinnington, A. Briscoe, Externally applied sensor for axisymmetric waves in a fluid filled pipe, J. Sound Vib. 173 (4) (1994) 503–516, http://dx.doi.org/10.1006/jsvi.1994.1243.
[19] J. Muggleton, M. Brennan, P. Linford, Axisymmetric wave propagation in fluid-filled pipes: wavenumber measurements in in vacuo and buried pipes, J. Sound Vib. 270 (1–2) (2004) 171–190, http://dx.doi.org/10.1016/S0022-460X(03)00489-9.
[20] ISO 1183-1, Plastics - Methods for determining the density of non-cellular plastics - Part 1: Immersion method, liquid pyknometer method and titration method, Standard, Brussels: CEN, 2012.
[21] X.-F. Pang, Water: Molecular Structure and Properties, World Scientific, 2013.
[22] J. Kubat, M. Rigdahl, M. Welander, Characterization of interfacial interactions in high density polyethylene filled with glass spheres using dynamic-mechanical analysis, J. Appl. Polym. Sci. 39 (7) (1990) 1527–1539, http://dx.doi.org/10.1002/app.1990.070390711.
[23] Y. Men, J. Rieger, H.-F. Endeler, D. Lilge, Mechanical α-process in polyethylene, Macromolecules 36 (13) (2003) 4689–4691, http://dx.doi.org/10.1021/ma0344902.
[24] K.-h. Nitta, M. Yamana, Poisson's ratio and mechanical nonlinearity under tensile deformation in crystalline polymers, in: J. Vicente (Ed.), Rheol. Open Access (2012) 113–132.
[25] R. Long, K. Vine, M.J.S. Lowe, P. Cawley, The effect of soil properties on acoustic wave propagation in buried iron water pipes, AIP Conf. Proc. 615 (1) (2002) 1310–1317, http://dx.doi.org/10.1063/1.1472947.
[26] G. Carter, C. Knapp, Coherence and its estimation via the partitioned modified chirp-z transform, IEEE Trans. Acoust. Speech Signal Process. 23 (3) (1975) 257–264.
[27] J.-L. Bertrand-Krajewski, F. Clemens-Meyer, M. Lepot, Metrology in urban drainage and stormwater management: Plug and pray, IWA Publishing, 2021.
[28] O. Scussel, A. Seçgin, M. Brennan, J. Muggleton, F. Almeida, A stochastic model for the speed of leak noise propagation in plastic water pipes, J. Sound Vib. 501 (2021) 116057, http://dx.doi.org/10.1016/j.jsv.2021.116057.
[29] Y. Gao, F. Sui, J.M. Muggleton, J. Yang, Simplified dispersion relationships for fluid-dominated axisymmetric wave motion in buried fluid-filled pipes, J. Sound Vib. 375 (2016) 386–402, http://dx.doi.org/10.1016/j.jsv.2016.04.012.
[30] M. Brennan, M. Karimi, J. Muggleton, F. Almeida, F.K. de Lima, P. Ayala, D. Obata, A. Paschoalini, N. Kessissoglou, On the effects of soil properties on leak noise propagation in plastic water distribution pipes, J. Sound Vib. 427 (2018) 120–133, http://dx.doi.org/10.1016/j.jsv.2018.03.027.
[31] A.W. Leissa, Vibration of Shells, National Aeronautics and Space Administration, Scientific and Technical Information Office, USGPO, Washington, 1973.
[32] J. Rose, Ultrasonic Guided Waves in Solid Media, Cambridge University Press, Cambridge, 2014, http://dx.doi.org/10.1017/CBO9781107273610.
[33] J.X. Liu, T.Y. Li, T.G. Liu, J. Yan, Vibration characteristic analysis of buried pipes using the wave propagation approach, Appl. Acoust. 66 (3) (2005) 353–364, http://dx.doi.org/10.1016/j.apacoust.2004.06.010.
[34] M.C. Junger, D. Feit, Sound, Structures, and their Interaction, second Ed., MIT Press, Cambridge, Massachusetts, 1986.
[35] C.A.F. De Jong, Analysis of Pulsations and Vibrations in Fluid-Filled Pipe Systems, (Doctoral Dissertation), Eindhoven University of Technology, Eindhoven, The Netherlands, 1994, http://dx.doi.org/10.6100/IR423649.
[36] COMSOL, Structural mechanics module user's guide, 2017.
[37] COMSOL, Acoustics module user's guide, 2017.